10-3-2018

Au@h-Al2O3 Analogic Yolk–Shell Nanocatalyst for Highly Selective Synthesis of Biomass-Derived D-xylonic Acid via Regulation of Structure Effects

Jiliang Ma
South China University of Technology

Zewei Liu
South China University of Technology

Junlong Song
Nanjing Forestry University

Linxin Zhong
South China University of Technology

Dequan Xiao
University of New Haven, DXiao@NewHaven.edu

See next page for additional authors

Publisher Citation

Ma, Jiliang, Zewei Liu, Junlong Song, Linxin Zhong, Dequan Xiao, Hongxia Xi, Xuehui Li, Run-Cang Sun, and Xinwen Peng (2018). "Au@ h-Al2O3 analogic yolk-shell nanocatalyst for highly selectively synthesis of biomass-derived D-xylonic acid via regulation of structure effect." Green Chemistry 20:5188-5195.

Comments

This is the authors' accepted manuscript of the article published in *Green Chemistry.* The published version can be found at http://dx.doi.org/10.1039/C8GC02618A

Authors

Jiliang Ma, Zewei Liu, Junlong Song, Linxin Zhong, Dequan Xiao, Hongxia Xi, Xuehui Li, Runcang Sun, and Xinwen Peng

Au@*h*-Al_2O_3 analogic yolk-shell nanocatalyst for highly selectively synthesis of biomass-derived D-xylonic acid via regulation of structure effect

Jiliang Ma,[a] Zewei Liu,[a,c] Junlong Song,[b] Linxin Zhong,*[a] Dequan Xiao,[d] Hongxia Xi,[c] Xuehui Li,[c] Runcang Sun *[e] and Xinwen Peng *[a]

[a] State Key Laboratory of Pulp and Paper Engineering, South China University of Technology, Guangzhou, China. 510641.

[b] Jiangsu Co-Innovation Center for Efficient Processing and Utilization of Forest Resources, Nanjing Forestry University, Nanjing, China.

[c] School of Chemistry and Chemical Engineering, South China University of Technology, Guangzhou, China.

[d] Center for Integrative Materials Discovery, Department of Chemistryand Chemical Engineering, University of New Haven, West Haven, CT 06516.

[e] Institute of Biomass Chemistry and Utilization, Beijing Forestry University, Beijing, China.

*Corresponding authors' E-mail: fexwpeng@scut.edu.cn (Xinwen Peng), lxzhong0611@scut.edu.cn (Linxin Zhong) and rcsun3@bjfu.edu.cn (Runcang Sun), Tel.: +86-020-87111860; Fax: +86-020-87111860.

Abstract

Selective oxidation of biomass-based monosaccharides into value-added sugar acids is highly desired, yet limited success of producing D-xylonic acid has been achieved. Here, we report an efficient catalyst system, Au nanoparticles anchoring on the inner wall of hollow Al_2O_3 nanospheres (Au@*h*-Al_2O_3), which could catalyze the selective oxidation of D-xylose into D-xylonic acid under base-free conditions. The mesoporous Al_2O_3 shell as adsorption sites first adsorbed D-xylose, the interface of Au nanoparticles and Al_2O_3 as active sites spontaneously dissociated O_2, and the exposed Au nanoparticles surface as catalytic sites drove the transformation. With this catalyst system, the valuable D-xylonic acid was produced with excellent yields in the aerobic oxidation of D-xylose. Extensive works showed that the Au@*h*-Al_2O_3 is an efficient catalyst with highly stability and recycling.

Key words: D-xylose · D-xylonic acid · Au@*h*-Al_2O_3 · structural effect regulation system · selective oxidation

Introduction

Use of biomass-derived feedstocks provides an environmentally friendly and sustainable route for the production of chemicals. Organic acid is a versatile, renewable chemical with a wide industrial application profile both as a solvent and as a building block.[1,2] It is also widely used in food, pharmaceutical, cosmetic, detergent, polymer, and textile.[3,4] Transformation of biomass into value-added organic acids is highly desired, but is still very limited owing to the lack of efficient catalytic system and method. Recently, monosaccharide oxidation (especially selective oxidation), as a crucial element of organic acid production, offers an attractive option on the conversion of biomass resources into chemicals and sugar acids.

D-Xylose, one of the main sugar units in hemicelluloses, is the second most abundant sugar in nature.[5] Many efforts have been made on utilizing of D-xylose by fermenting[6] or other processes to obtain fuels and chemicals.[7-10] Among these products, D-xylonic acid is one of the top 30 high-value chemicals identified by the US Department of Energy. It is a key compound for the preparation of 1,2,4-butanetriol or energetic materials 1,2,4-butanetriol trinitrate.[11] Currently, as a concrete additive, D-xylonic acid can effectively improve concrete dispersion.[12] Furthermore, D-xylonic acid can be used as an efficient biocatalyst for organic transformations.[13] Other applications of D-xylonic acid have been reported in food, pharmaceutical, and agriculture.[14,15] Therefore, innumerous scientists have devoted to themselves to the synthesis of D-xylonic acid research. Among all the literatures, microbial production of D-xylonic acid plays a significant role in the synthesis of D-xylonic acid. As early as 1946, Lockwood and Nelson reported that the production of D-xylonic acid could occur in the Pseudomonas.[16] Later, a lot of studies have found that $_{\mathrm{D}}$-xylonic acid could be produced in the oxidative metabolism of $_{\mathrm{D}}$-xylose by some archaea and bacteria.[9, 17-20] But until now, commercial production of $_{\mathrm{D}}$-xylonic acid has not been developed, reflecting the current limited market for $_{\mathrm{D}}$-xylonic acid. The reason lies in two facts: the one is that many others oxidizing enzymes are produced by bacteria strains which directly contribute to the conversion of other sugars present in lignocellulosic hydrolysates, the other is that the engineered yeast strains have low $_{\mathrm{D}}$-xylonic acid accumulation rate and yield.[9] Besides, industrial scale production of $_{\mathrm{D}}$-xylonic acid needs the high cost of peptone and/or yeast extract media as nitrogen sources, which decide that the production methods are impractical. Furthermore, although the application of chemical synthesis in industrial production is widespread, few studies have been reported for the synthesis of $_{\mathrm{D}}$-xylonic acid by chemical synthesis.

Au-based catalysts are found to be superior to Pt, Pd and Pt/Pd bimetallic catalysts for the oxidation of glucose to gluconic acid,[21] as Au nanoparticles (NPs) have low sensitivity to oxygen poisoning and high activity in a wide range of pH values. However, the free Au NPs with high surface energy are easy to agglomerate, which affect its activity. To avoid this drawback, functional supports with a strong interaction with Au,[22-26] pores[27-30] and core/yolk-shell architecture[31-33] are developed to improve the stability of Au NPs. The core/yolk-shell architecture featured the advantages of high permeability, low density, large surface area, multifunctionality, and high loading capacity,[31, 34-38] Furthermore, modification of the core/yolk-shell structure to give a nanocatalyst with metal NPs embedded on its inner wall can not only improve the stability of metal NPs, but also generate a synergistic effect on the interface between the metal NPs and the shell.[39, 40]

Herein, we report a new catalyst of Au NPs anchoring on the inner wall of mesoporous hollow Al_2O_3 nanospheres, prepared via the technique of core/yolk-shell architecture. The Au@*h*-Al_2O_3 catalyst can selectively oxidize $_D$-xylose to $_D$-xylonic acid. The correlation between the unique structure and catalytic activity of Au@*h*-Al_2O_3 was revealed through comparative experiments. The adsorption sites were investigated by a technique called quartz crystal microbalance with dissipation monitoring (QCM-D) and DFT calculations. The active sites for the spontaneous dissociation of O_2 were studied by DFT calculations. The catalytic sites of Au@*h*-Al_2O_3 were verified by the comparison experiment of sulfhydryl coated surface of Au NPs.

Results and discussion

The synthetic scheme of the Au@*h*-Al_2O_3 is shown in Fig. 1. A soap-free emulsion polymerization method was adopted to prepare a core/shell structure of PS-*co*-P4VP,[41] which was then used as scaffold for the immobilization of Au NPs. The dispersed Au NPs were then anchored onto the PS-*co*-P4VP core/shell microspheres by coordination of Au^{3+} (from $HAuCl_4$) with the P4VP shell first and then by reduction with $NaBH_4$.[41] Afterwards, uniform layers were gradually growing onto the surface of Au@PS-*co*-P4VP by controlling the precipitation process in a buffer solution of formic acid-ammonium formate.[42] Finally, the resultant NPs were calcined to remove PS-*co*-P4VP and allow the Au NPs to be distributed on the inner wall of the hollow Al_2O_3 sphere. In this process, PS-*co*-P4VP microspheres played a dual role, a scaffold for immobilization of dispersed Au NPs[41] and a template for the synthesis of Al_2O_3 coating.

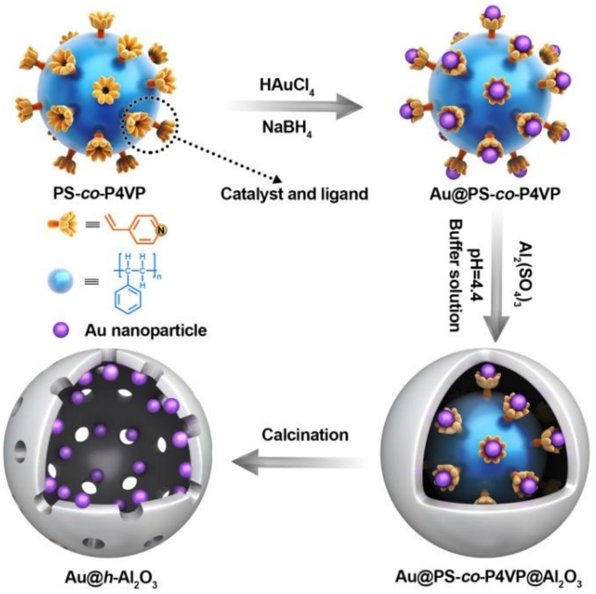

Fig. 1 Schematic illustration of the synthetic route of Au@*h*-Al_2O_3.

The morphology and chemical composition of the intermediate and Au@*h*-Al_2O_3 were first characterized by scanning electron microscope (SEM). As shown in Fig. 2A, the pure PS-*co*-P4VP microspheres with an average size of about 490 nm were observed. As compared with the PS-*co*-P4VP microspheres, Au@PS-*co*-P4VP microspheres showed no significant difference on morphology and size (Fig. 2B). The elements of Au@PS-*co*-P4VP were mainly Au, C, O and N (the inset of Fig. 2B), indicating that Au NPs were successfully deposited on the surface of PS-*co*-P4VP. After the precipitation of Al_2O_3 on the surface of Au@PS-*co*-P4VP microspheres (using $Al_2(SO_4)_3$ as the precursor of Al_2O_3), a thin shell was coated to produce Au@PS-*co*-P4VP@Al_2O_3 microspheres, which was confirmed by a slight increase in the size from 490 to 510 nm (Fig. 2C, 2H). The elemental mapping of O, Al, Au, C and N (Fig. 2I-2M) further evidenced the successful preparation of Au@PS-*co*-P4VP@Al_2O_3 microspheres. After Au@PS-*co*-P4VP@Al_2O_3 NPs were calcined at 550 ^{o}C, the polymeric template was removed, and Au NPs were left on the inner wall of hollow Al_2O_3 sphere, producing Au@*h*-Al_2O_3 (Fig. 2D and

Supporting Information Fig. S1). Only Al, Au and O were observed in the EDX area scanning of Au@*h*-Al_2O_3, which indicates that the cavity structure was achieved after the calcination (Fig. 2E-G).

The transmission electron microscopy (TEM) image of pure PS-*co*-P4VP microspheres in Fig. S2A is consistent with the SEM results. In the TEM images of Fig. S2B, the Au@PS-*co*-P4VP@Al_2O_3 microspheres with a diameter of ~510 nm. The inter bright spots represent the PS-*co*-P4VP core; the dark spots indicate the Au NPs, while the peripheral dark circle corresponds to Al_2O_3 shell. After PS-*co*-P4VP core was removed, the shell (of 10 nm in thickness) and the cavity were clearly observed by TEM and STEM (Fig. 3A and 3B); and Au NPs with a diameter of ~1.87 nm were observed on the inner wall of Al_2O_3 microspheres (the inset in Fig. 3B). Besides the diameter of Au NPs slightly increased from 1.87 to 2.20 nm (Supporting Information Fig. S3C), and no significant difference in size was observed for Au@*h*-Al_2O_3 after being used for 10 times (Supporing Information Fig. S3A, S3B and S4), indicating the high stability of Au@*h*-Al_2O_3. The Au element analyzed with XPS is shown in Fig. 3D. The signal of Au 4f can be resolved into two peaks. The binding energies of Au $4f_{5/2}$ and Au $4f_{7/2}$ locating at 87.7 and 83.9 eV indicate Au^0, while the 89.6 and 86.3 eV demonstrate Au_2O_3, respectively.[43] There was no significant difference in Au valence for Au@*h*-Al_2O_3 before and after catalysis for D-xylose oxidation. For the freshly prepared Au@*h*-Al_2O_3, the peaks locating at 83.9 and 87.5 eV reveal only the valence of Au species. After being used for the synthesis of D-xylonic acid, the peaks shift slightly to the lower binding energies at 83.5 and 87.3 eV (Supporting Information Fig. S5), respectively, indicating that the valence of Au species did not change much during the catalytic oxidation process. In addition, the difference in O 1s and Al 2p spectra for Au@*h*-Al_2O_3 was not significant before and after being used for D-xylose oxidation (Supporting Information Fig. S6). The Au contents determined by ICP-MS were 2.80 wt% and 2.49 wt% for Au@*h*-Al_2O_3 before use and after 10 catalytic cycles, respectively, indicating that Au@*h*-Al_2O_3 has excellent stability (Supporting Information Table S1). Fig. S7A shows the HAADF-STEM spectrum of Au@*h*-Al_2O_3. The white spots indicate the Au NPs and the peripheral white circle corresponds to the Al_2O_3 shell. The elemental mapping of O, Al and Au in Au@*h*-Al_2O_3 are shown in Fig. S7B-D, demonstrating the actual distributions of O, Al, and Au elements in the catalyst. Fig. 3C shows the HRTEM image of Au@*h*-Al_2O_3. There were mainly two types of lattice fringes with interplanar spacing of 2.32 and 2.0 Å, corresponding to (111) and (200) crystal planes of Au NPs, respectively. The inset in Fig. 3C shows the diffraction pattern of Au NPs. To illustrate the position of Au NPs in Au@*h*-Al_2O_3, a STEM spectrum of Au NP is given in Fig. S8A; then a line scan of the Au NP is shown in Fig. S8B, which gives a preliminary explanation of the position of Au NPs in Au@*h*-Al_2O_3. Fig. 3F shows the XRD pattern of Au@*h*-Al_2O_3 catalyst. Au@*h*-Al_2O_3 displays a good crystallinity and the diffraction peaks at $2\theta = 38.27^\circ$, 44.6°, 64.68° and 77.55° were assigned to (111), (200), (220) and (311) reflections of the gold lattice, well agreeing with the results from Fig. 3C. The 10th reused Au@*h*-Al_2O_3, Au/Al_2O_3 and other Au catalysts (Supporting Information Fig. S4F and S9a-d) also showed the similar diffraction peaks.

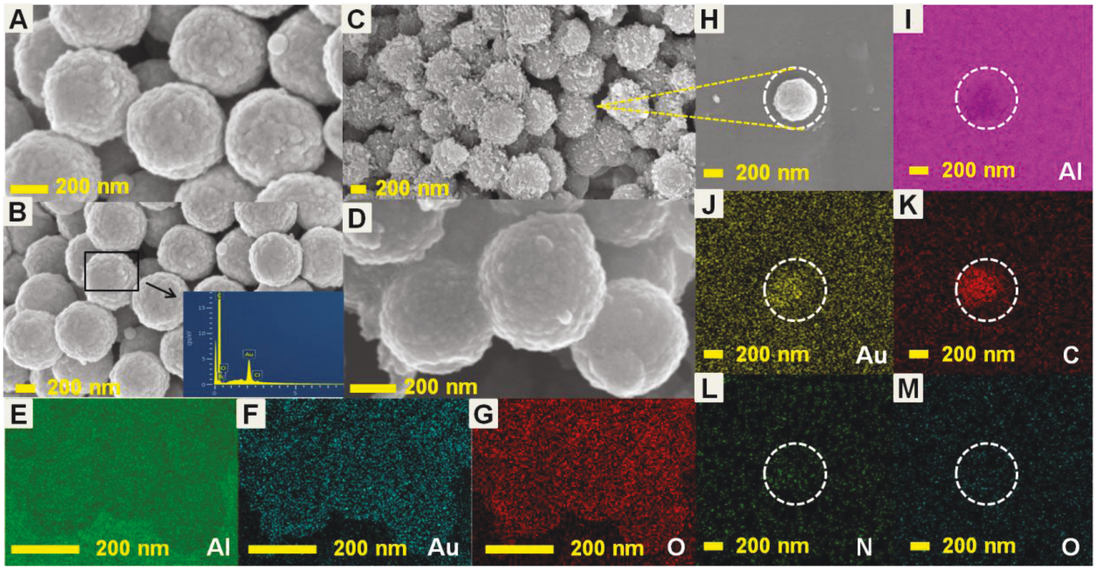

Fig. 2 SEM of PS-*co*-P4VP (A), Au@PS-*co*-P4VP (B) (the inset is the EDX of Au@PS-*co*-P4VP), Au@PS-*co*-P4VP@Al_2O_3 (C, H), Au@*h*-Al_2O_3 (D) and element mapping images of Au@*h*-Al_2O_3: Al element (E), Au element (F), and O element (G), the element mapping images of Au@PS-*co*-P4VP@Al_2O_3: Al element (I), Au element (J), C element (K), N element (L) and O element (M).

To further determine the distribution patterns of Al, O and Au in Au@*h*-Al_2O_3, Au@*h*-Al_2O_3 with 10 times $HAuCl_4$ addition was prepared and the obtained products were named Au@*h*-Al_2O_3-10. Besides an obvious increase in diameters of Au NPs (the inset in Supporting Information Fig. S10B), no significant difference was observed between Au@*h*-Al_2O_3-10 and Au@*h*-Al_2O_3 (Supporting Information Fig. S10A-E). The elemental mapping of Au@*h*-Al_2O_3-10 in Fig. S10F-H gave a clear distribution of O, Al and Au. The TEM and STEM of the cross section diagram of Au@*h*-Al_2O_3-10 visually showed the distribution of Au NPs (Fig. 3E, 3H and Supporting Information Fig. S11). The line scan spectrum and elemental mapping of the cross section diagram of Au@*h*-Al_2O_3-10 further presented the actual distributions of O, Al, and Au elements (Fig. 3G and 3I-3K). All the results demonstrated that Au NPs are well distributed on the inner wall of the Al_2O_3 hollow sphere.

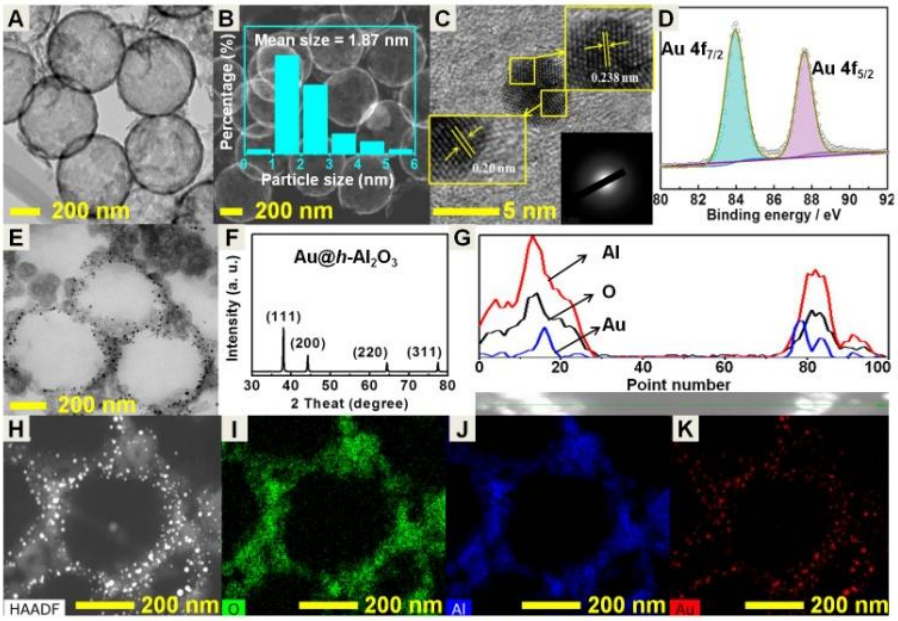

Fig. 3 TEM and STEM of Au@*h*-Al_2O_3 (A, B). The inset B is the size distributions of Au NPs from 300 particles. (C) High-resolution TEM image of Au@*h*-Al_2O_3 (the inset is the diffraction patterns of Au NPs). (D) Au 4f spectra for Au@*h*-Al_2O_3. (E) TEM of the cross section diagram of Au@*h*-Al_2O_3-10. (F) The XRD pattern of Au@*h*-Al_2O_3. (G) The line scan of cross section diagram of Au@*h*-Al_2O_3-10. (H) STEM-HAADF image of the cross section diagram of Au@*h*-Al_2O_3-10 and element mapping images: (I) O element, (J) Al element, and (K) Au element.

The N_2 sorption isotherms of Au/Al_2O_3, Au@PS-*co*-P4VP@Al_2O_3 and Au@*h*-Al_2O_3 exhibit type IV isotherm patterns (Supporting Information Fig. S12), suggesting the presence of mesopores in these materials. Compared to Au/Al_2O_3 and Au@PS-*co*-P4VP@Al_2O_3, Au@*h*-Al_2O_3 showed more uniform and well-developed mesopores with a diameter of 2.19 nm, favoring the diffusion of reactants and products in and out of the catalyst. The BET results showed that the surface area of Au@*h*-Al_2O_3 increases from 10.09 to 100.45 m^2/g after removing PS-*co*-P4VP, indicating a higher contact area between D-xylose and Au@*h*-Al_2O_3. Fig. S13 shows no significant difference in the thermal weight loss between Au@*h*-Al_2O_3 and Au/Al_2O_3, demonstrating that the catalysts have a good thermostability. Although weight loss occurs to Au@PS-*co*-

P4VP@Al_2O_3 when the temperature was higher than 350 °C, it has no impact on the aerobic oxidation of D-xylose because the reaction was carried out in the temperature range of 100-160 °C.

Prior to comprehensively investigate the catalytic activity of Au@*h*-Al_2O_3 on the aerobic oxidation of D-xylose to D-xylonic acid, the affinities of D-xylose to various surfaces (Al_2O_3, silica, and gold) were compared by a technique of quartz crystal microbalance with dissipation monitoring (QCM-D). Fig. S14 shows that the frequency change of Al_2O_3 surface is -7.3 Hz after water rinsing, which is equivalant to 129.2 mg/m^2, higher than those of silica (-1.4 Hz and 24.8 mg/m^2) and gold (-4.9 Hz and 86.7 mg/m^2) surfaces. The results suggest that Al_2O_3 has a much stronger affinity to D-xylose than silica and gold.

The adsorption energy of D-xylose on Al_2O_3 was calculated by DFT methods using DMOL3 module from Materials Studio 2017.[44] A model of the dehydrated Al_2O_3 (110) surface (Fig. 4A), the same as that used by Falamaki and co-workers,[45] was chosen to investigate the interactions between D-xylose and the Al_2O_3 crystal. The adsorption energy of D-xylose on Al_2O_3 (110) was -70 kJ/mol. In addition, the dissociation energy O_2 on the interface of Au NPs and Al_2O_3 shell was also calculated by DFT as -245.68 kJ/mol (Fig. 4B and 4C), suggesting that the O_2 molecule can be dissociated spontaneously on the interface of Au NPs and Al_2O_3 shell. The generated negative oxygen ion is expected to react with water to produce oxidizing substances. These results indicate that it is feasible to synthesize D-xylonic acid from D-xylose catalyzed by Au@*h*-Al_2O_3.

For the aerobic oxidation of D-xylose to D-xylonic acid catalyzed by Au@*h*-Al_2O_3, the reaction was carried out at different temperatures (100-

160 ^{o}C) in the presence of O_2 (3.0 MPa). As shown in Table S2, the yield of D-xylonic acid first significantly increased from 38.6% to 83.3% when reaction temperature was raised from 100 to 130 °C (Supporting Information Table S2, entries 1-4), and then gradually decreased as the temperature reached 160 °C (Supporting Information Table S2, entries 4-7). The decreasing yield may be due to the production of byproducts (e.g., formic acid, acetic acid and lactic acid) at high temperature. The selectivities of D-xylonic acid increased first and then decreased with the increasing temperature (Fig. 4E), while the conversion of D-xylose increased with the increase of temperature (Fig. 4F), implying endothermic nature of the overall reaction. Thus, 130 °C was chosen as the optimal reaction temperature. After that, the reaction was tested under different O_2 pressure. It was found that only 14.7% of D-xylonic acid was obtained when air was used as oxidizer (Supporting Information Table S3, entry 1). As the O_2 pressure increased to 3.0 MPa, the yield remarkably increased from 14.7% to 83.3% (Supportiing Information Table S3, entries 1-6). A slight decrease of D-xylonic acid yield (79.6%) (Supporting Information Table S3, entry 7), however, was observed when O_2 pressure increased to 4.0 MPa. The selectivity of D-xylonic acid under different O_2 pressure also showed similar change to that of the yield of D-xylonic acid, and the conversion of D-xylose increased with the increase of O_2 pressure (Supporting Information Fig. 4E and 4F).

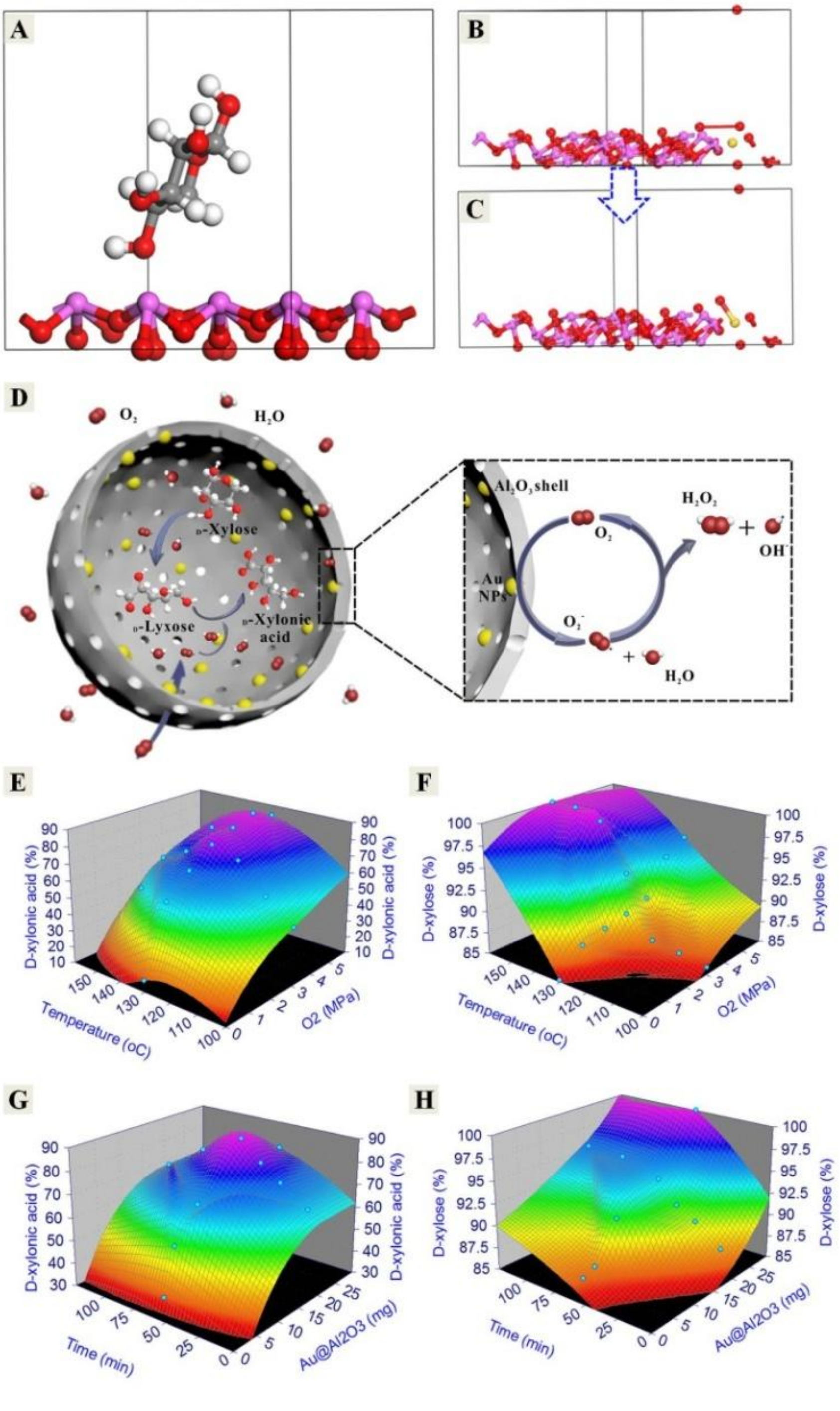

Fig. 4 The model of D-xylose adsorption energy on Al_2O_3 (110) (A) and O_2 dissociation energy on the interface of Au and Al_2O_3 in Au@*h*-Al_2O_3 (B and C) calculated by DFT (grey: C, white: H, pink: Al, red: O, yellow: Au). (D) Proposed reaction mechanism for the base-free oxidation of D-xylose to D-xylonic acid catalyzed by Au@*h*-Al_2O_3 (left) and oxygen dissociation reaction mechanism (right). The selectivity of D-xylonic acid (E) and conversion of D-xylose catalyzed (F) by Au@*h*-Al_2O_3 under different temperatures and oxygen pressures. The selectivity of D-

xylonic acid (G) and conversion of D-xylose (H) catalyzed by Au@*h*-Al_2O_3 under different reation times and catalyst dosages.

The dosage (relative to 0.25 g D-xylose) of Au@*h*-Al_2O_3 also played an important role in the aerobic oxidation of D-xylose to D-xylonic acid. The yield of D-xylonic acid increased with increasing dosage of Au@*h*-Al_2O_3 (Supporting Information Table S4, entries 1-4). An increase in dosage from 20 to 30 mg, however, did not lead to a significant increase in the yield of D-xylonic acid (Supporting Information Table S4, entries 4-5). It is possible that D-xylose molecules adsorbed on the Al_2O_3 shell became unstable species (more active), which reduced the activation energy of the reaction. Similar trend was observed for the selectivity of D-xylonic acid, as shown in Fig. 4G. The conversion of D-xylose increased with increasing dosage of Au@*h*-Al_2O_3 (Fig. 4H). Therefore, 20 mg of Au@*h*-Al_2O_3 is optimal for this reaction. Furthermore, the effect of reaction time on the oxidation of D-xylose was also examined. With the growth of reaction time, both the yield (Supporting Information Table S5, entries 1-4) and selectivity (Fig. 4G) increased, and then decreased after 60 min. This phenomenon might be due to the generation of byproduct (e.g., formic acid and acetic acid) from the produced D-xylonic acid with increasing reaction time (Supporting Information Table S5, entries 4-6). The conversion of D-xylose also increased with the increase of reaction time (Fig. 4H). Furthermore, the D-xylonic acid yield and the conversion of D-xylose decreased slightly from 83.3% to 80.5% and from 93.8% to 92.8% in the tenth recycling run, respectively. Thus, Au@*h*-Al_2O_3 is highly stable and recyclable (Supporting Information Fig. S15).

Table 1. Base-free oxidation of D-xylose with structurally different Al_2O_3-based Au catalyst.[a]

Entry	Al_2O_3-based Au catalyst	D-Xylonic acid (%)
1	Au/Al_2O_3	21.6
2	Au@PS-*co*-P4VP@Al_2O_3	17.2
3	Au@*h*-Al_2O_3	83.3
4	Au-SH-$(CH_2)_3$-$Si(OCH_3)_3$/Al_2O_3	9.6
5	Au-SH-$(CH_2)_3$-$Si(OCH_3)_3$@PS-*co*-P4VP@Al_2O_3	5.2
6	Au-SH-$(CH_2)_3$-$Si(OCH_3)_3$@*h*-Al_2O_3	13.0

[a] Typical reaction conditions: D-xylose (0.25 g), O_2 (3.0 MPa), water (25 mL), Al_2O_3-based Au catalyst (20 mg), 130 °C, 60 min.

To better understand our catalyst, the catalytic efficiency of Au@*h*-Al_2O_3 was compared with those catalysts that prepared in the literatures. A series of experiments were carried out at the optimal condition and the results are presented in Table S6. Although there was no significant difference in the conversion of D-xylose between Au@*h*-Al_2O_3 and other catalysts, the yield of D-xylonic acid (thus selectivity) was different. The yield of D-xylonic acid catalyzed by Au@*h*-Al_2O_3 was significantly higher than those of other catalysts (Au/SBA-15[46]: 16.8%, Au@PS-*co*-P4VP: 11.4%, SiO_2-SH-Au: 1.6%, C-SH-Au: 10.8%). Furthermore, the effect of morphology of catalyst on the oxidation of D-xylose was also investigated. As shown in Table 1, the yield of D-xylonic acid catalyzed by Au/Al_2O_3 was higher than that catalyzed by Au@PS-*co*-P4VP@Al_2O_3, while Au@*h*-Al_2O_3 showed a even higher yield than Au/Al_2O_3[47], implying that the Au@*h*-Al_2O_3 catalyst with special structure can effectively promote the formation of D-xylonic acid. All these results suggest that the Au@*h*-Al_2O_3 has very high catalytic activity for the aerobic oxidation of D-xylose into D-xylonic acid compared to other catalysts. In addition, the possible reaction pathways and descriptions was given in supporting informatin (Table S7, Fig. S16 and Fig. S17)

To determine the catalytic sites of Au@*h*-Al_2O_3, we used 3-mercaptopropyltrimethoxysilane to treat the Au@*h*-Al_2O_3, and the exposed Au NPs surface was covered with sulfhydryl groups. The resulting Au-SH-$(CH_2)_3$-Si$(OCH_3)_3$@*h*-Al_2O_3 (Supporting Information Fig. S18) was used to catalyze D-xylose. Only 13.0% yield of D-xylonic acid was obtained, which well agrees with the results of Table S6 (entries 3 and 4). The phenomenon suggested that the catalytic sites of Au@*h*-Al_2O_3 were the exposed Au NPs surface. Hence, we proposed a plausible reaction mechanism of synthesis of D-xylonic acid from D-xylose catalyzed by Au@*h*-Al_2O_3 (Fig. 4D). According to the early reports,[48] hydrogen peroxide, as a byproduct, was produced from the aerobic oxidation of glucose to gluconic acid. The hydrogen peroxide acted as an oxidant to oxidize glucose. In this work, our DFT calculations showed that the O_2 molecule was dissociated spontaneously on the interface of Au NPs and Al_2O_3 (Fig. 4B and 4C), and D-xylose was preferably adsorbed on Al_2O_3 (Fig. 4A and Supporting Information Fig. S14). The resulting negative oxygen ion can react with water to produce O_2, hydrogen peroxide and hydroxyl ions (Fig. 4D, right panel). Then the isomerization reaction between D-xylose and chain intermediate may occur in the presence of hydroxyl ions. Finally, the chain intermediate was oxidized by hydrogen peroxide to produce D-xylonic acid.

Conclusions

In summary, we demonstrated a highly effective chemical method for the synthesis of D-xylonic acid from D-xylose, catalyzed by Au@*h*-Al_2O_3. The catalytic oxidation of D-xylose was facile with high yields. The correlation between the unique structure and catalytic activity of Au@*h*-Al_2O_3 was revealed through comparative experiments. The Al_2O_3 shell played a dual role in the stabilization of Au NPs and the adsorption of D-xylose. DFT calculations revealed that the unique structure between Au NPs and Al_2O_3 provided a synergism for spontaneous dissociation of O_2, and hence promoted the formation of D-xylonic acid. At the condition of 130 °C, 3.0 MPa O_2 and 60 min reaction time, the D-xylose conversion was 93.8%, and the D-xylonic acid yield was 83.8%. Compared with other Au supported catalysts (e.g. Au/SBA-15, SiO_2-SH-Au, Au@PS-*co*-P4VP, etc.), Au@*h*-Al_2O_3 showed selectivity toward the production of D-xylonic acid. Au@*h*-Al_2O_3 was stable after 10 rounds of catalytic recycling. This work provides a new facile route to selectively oxidize monosaccharides into value-added sugar acids such as D-xylonic acid, using a type of hermit crab typological nanocatalyst Au@*h*-A_2O_3.

Experimental

Synthesis of Au@*h*-Al_2O_3 nanocatalyst

The styrene was pretreated before use. First, a certain amount of commercially available styrene was added into 10% sodium hydroxide solution, and the system was placed stably for 10 min at 4 °C. The process was replicated for 3 times. Thereafter, the styrene was washed with water and dried with anhydrous magnesium sulfate overnight. Finally, the pure styrene was obtained by vacuum distillation and kept at 4 °C.

The polystyrene-*co*-poly(4-vinylpyridine) (PS-*co*-P4VP) core-shell microspheres were synthesized by one-stage, soap-free emulsion polymerization.[49] Typically, 80 mmol of 4-vinylpyridine was mixed with 360 mL of water at room temperature, then 160 mmol of styrene was added to the above system under magnetic stirring. The mixture was stirred vigorously for another 30 min at room temperature. Thereafter, 1.30 g of $K_2S_2O_8$ was added into the reaction system, and the pH of the mixture was adjusted to 7 with 0.1 mol/L HCl aqueous solution. The reaction system was then filled with nitrogen and carried out at 80 °C for 24 h under vigorous stirring conditions. Finally, the excessive volume of 0.1 mol/L NaOH aqueous solution was injected into the above colloidal dispersion, and the obtained precipitates were washed with deionized water and then dried in a vacuum at 50 °C overnight.

0.480 g PS-*co*-P4VP was dispersed in $HAuCl_4$ aqueous solution and stirred at room temperature for 17 h. After that, the pH of the mixture was adjusted to 7 with 0.1 mol/L NaOH aqueous solution, and then a 5-fold excess volume of 0.1 mol/L $NaBH_4$ aqueous solution was added drop wise with vigorous stirring. The obtained Au@PS-*co*-P4VP core-shell microspheres were collected by centrifugation, washed thrice with deionized water, and dried in a vacuum at 80 ^{o}C.

A certain volume of formic acid-ammonium formate buffer solution (pH = 4.4) was first prepared. Then, a certain amount of Au@PS-*co*-P4VP core-shell microspheres and aluminum sulfate were added and dispersed by ultrasound for 15 min. The system was carried out at 70 ^{o}C for 2 h with vigorous stirring. The obtained Au@PS-*co*-P4VP@Al_2O_3 was collected by centrifugation, washed with deionized water and oven-dried at 80 ^{o}C overnight. The Au@*h*-Al_2O_3 was obtained by calcinating

Au@PS-*co*-P4VP@Al_2O_3 at 550 °C for 4 h. Changing the concentration of aluminum salts can easily tune the thickness of aluminum oxide shell.

Activity Tests. The catalytic synthesis of D-xylonic acid were carried out in a 60 mL Teflon-lined stainless-steel autoclave. In a typical procedure, 0.25 g D-xylose was dissolved in 25 mL water, and then a certain amount of Au@*h*-Al_2O_3 was added into the solution and dispersed by ultrasound for 10 min. Then oxygen was purged into the reactor for three times before the reactor being sealed and pressurized with oxygen. The reaction was then heated to a required temperature for different times under constant stirring (1000 rpm). After the completion of the reaction, the autoclave was immersed in a water bath to cool down, and the oxygen was expelled from the stainless-steel autoclave at the same time. Finally, the sample was immediately syringed out, filtered and analyzed by high-performance liquid chromatography (HPLC, Agilent 1260 series) with a UV detector.

Conflicts of interest

The authors declare no conflict of interest.

Acknowledgements

We wish to thank for the Natural Science Foundation of China (31430092, 21506068, 21736003, 21576094), Guangdong Natural Science Funds for Distinguished Young Scholar (2016A030306027, 2017A030306029), Tip-top Scientific and Technical Innovative Youth Talents of Guangdong Special Support Program (2015TQ01C488), Guangdong Natural Science Foundation (2017A030313130), State Key Laboratory of Pulp and Paper Engineering and Fundamental Research Funds for the Central

Universities. We also thank to the Qian Liu from shiyanjia lab (www.shiyanjia.com) for the XPS analysis.

Notes and references

1 Z. L. Zhang and G. W. Huber, *Chem. Soc. Rev.*, 2018, **47**, 1351-1390.

2 V. G. Goz, I. Pinter, V. Harmat and A. Perczel, *Eur. J. Org. Chem.*, 2018, **3**, 355-361.

3 J. J. Liu, J. H. Li, H. D. Shin, L. Liu, G. C. Du, and J. Chen, *Bioresource Technol.*, 2017, **239**, 412-421.

4 S. P. N. Ayudthaya, A. H. P. van de Weijer, A. H. van Gelder, A. J. M. Stams, W. M. de Vos and C. M. Plugge, *Biotechnol. Biofuels,* 2018, **11**, 1-15.

5 M. Toivari, M. L. Vehkomaki, Y. Nygard, M. Penttila, L. Ruohonen and M. G. Wiebe, *Bioresource Technol.*, 2013, **133**, 555-562.

6 J. H. Van Vleet and T. W. Jeffries, *Curr. Opin. Biotechnol.*, 2009, **20**, 300-306.

7 S. J. Kim, H. J. Sim, J. W. Kim, Y. G. Lee, Y. C. Park and J. H. Seo, *Bioresource Technol.*, 2017, **245**, 1551-1557.

8 H. X. Fu, L. Yu, M. Lin, J. F. Wang, Z. L. Xiu and S. T. Yang, *Metab. Eng.*, 2017, **40**, 50-58.

9 H. Liu, K. N. G. Valdehuesa, G. M. Nisola, K. R. M. Ramos and W. J. Chung, *Bioresource Technol.*, 2012, **115**, 244-248.

10 J. S. Martin del Campo, J. Rollin, S. Myung, Y. Chun, S. Chandrayan, R. Patino, M. W. W. Adams and Y. H. P. Zhang, *Angew. Chem. Int. Edit.*, 2013, **52**, 4587-4590.

11 W. Niu, M. N. Molefe and J. W. Frost, *J. Am. Chem. Soc.*, 2003, **125,** 12998-12999.

12 B. W. Chun, B. Dair, P. J. Macuch, D. Wiebe, C. Porteneuve and A. Jeknavorian, *Appl. Biochem. Biotech*., 2006, **129**, 645-658.

13 J. L. Ma, L. X. Zhong, X. W. Peng and R. C. Sun, *Green Chem*., 2016, **18**, 1738-1750.

14 Y. Tomoda, A. Hanaoka, T. Yasuda, T. Takayama, A. Hiwatashi, Y. Tomota, T. Hanaoka, S. Takayama and A. Hiwatari, *US Patent*, 2004, 2004131737-A1.

15 P. Pujos, M. H. Jijakli, P. Philippe, M. H. Jujakli and M. Haissam Jujakli, *Patent*, 2006, WO2006032530-A1.

16 L. B. Lockwood, G. E. Nelson, *J. Bacteriol*., 1946, **52**, 581-596.

17 Y. Nygard, M. H. Toivari, M. Penttila, L. Ruohonen, M. G. Wiebe, *Metab. Eng*., 2011, **13**, 383-391.

18 M. H. Toivari, L. Ruohonen, P. Richard, M. Penttila, M. G. Wiebe, *Appl. Microbiol. Biot*., 2010, **88**, 751-760.

19 A. S. Dahms, *Biochem. Biophys. Res. Commun*., 1974, **60**, 1433-1439.

20 N. Tenhaef, C. Brusseler, A. Radek, R. Hilmes, P. Unrean, J. Marienhagen, S. Noack, *Bioresource. Technol*., 2018, **268**, 332-339.

21 S. Biella, L. Prati and M. Rossi, *J. Catal.*, 2002, **206**, 242-247.

22 H. Sakamoto, J. Imai, Y. Shiraishi, S. Tanaka, S. Ichikawa and T. Hirai, *ACS Catal*., 2017, **7**, 5194-5201.

23 S. J. Kim, S. J. Choi, J. S. Jang, H. J. Cho, W. T. Koo, H. L. Tuller and I. D. Kim, *Adv. Mater.*, 2017, **29**, 1-9.

24 J. F. Yu, Q. Wang, D. O'Hare and L. Y. Sun, *Chem. Soc. Rev.*, 2017, **46**, 5950-5974.

25 D. M. Meng, Q. Xu, Y. L. Jiao, Y. Guo, Y. L. Guo, L. Wang, G. Z. Lu and W. C. Zhan, *Appl. Catal. B-environ.*, 2018, **221**, 652-663.

26 M. Baya, U. Belio, I. Fernandez, S. Fuertes and A. Martin, *Angew. Chem. Int. Edit.*, 2016, **55**, 6978-6982.

27 J. Su, C. L. Xie, C. Chen, Y. Yu, G. Kennedy, G. A. Somorjai and P. D. Yang, *J. Am. Chem. Soc.*, 2016, **138**, 11568-11574.

28 J. B. Song, F. Wang, X. Y. Yang, B. Ning, M. G. Harp, S. H. Culp, S. Hu, P. Huang, L. M. Nie, J. Y. Chen and X. Y. Chen, *J. Am. Chem. Soc.*, 2016, **138**, 7005-7015.

29 M. T. Zhao, K. Yuan, Y. Wang, G. D. Li, J. Guo, L. Gu, W. P. Hu, H. J. Zhao and Z. Y. Tang, *Nature*, 2016, **539**, 76-80.

30 M. A. Khalily, H. Eren, S. Akbayrak, H. H. Susapto, N. Biyikli, S. Ozkar and M. O. Guler, *Angew. Chem. Int. Edit.*, 2016, **55**, 12257-12261.

31 X. Q. Liu, J. Iocozzia, Y. Wang, X. Cui, Y. H. Chen, S. Q. Zhao, Z. Li and Z. Q. Lin, *Energy Environ. Sci.*, 2017, **10**, 402-434.

32 B. Cai, R. Hubner, K. Sasaki, Y. Z. Zhang, D. Su, C. Ziegler, M. B. Vukmirovic, B. Rellinghaus, R. R. Adzic and A. *Angew. Chem. Int. Edit.*, 2018, **57**, 2963-2966.

33 S. Wu, J. Dzubiella, J. Kaiser, M. Drechsler, X. H. Guo, M. Ballauff and Y. Lu, *Angew. Chem. Int. Edit.*, 2012, **51**, 2229-2232.

34 L. S. Lin, X. Y. Yang, Z. J. Zhou, Z. Yang, O. Jacobson, Y. J. Liu, A. Yang, G. Niu, J. B. Song, H. H. Yang and X. Y. Chen, *Adv. Mater.*, 2017, **29**, 1-9.

35 J. J. Wei, K. Niikura, T. Higuchi, T. Kimura, H. Mitomo, H. Jinnai, Y. Joti, Y. Bessho, Y. Nishino, Y. Matsuo and K. Ijiro, *J. Am. Chem. Soc.*, 2016, **138**, 3274-3277.

36 C. Wu, P. Kopold, P. A. van Aken, J. Maier and Y. Yu, *Adv. Mater.*, 2017, **29**, 1-7.

37 G. D. Park, J. K. Lee and Y. C. Kang, *Adv. Funct. Mater.*, 2017, **7**, 1-9.

38 M. B. Gawande, A. Goswami, T. Asefa, H. Z. Guo, A. V. Biradar, D. L. Peng, R. Zboril and R. S. Varma, *Chem. Soc. Rev.*, 2015, **44**, 7540-7590.

39 R. J. Ren, L. Q. Xu, L. Zhu, X. Y. Wang, X. J. Ma, D. B. Wang, *ACS Appl. Mater. Inter.*, 2018, **10**, 11642-11651.

40 J. W. Feng, J. Liu, X. Y. Cheng, J. J. Liu, M. Xu, J. T. Zhang, *Adv. Sci.*, 2018, **5**, 1-7.

41 F. Wen, W. Q. Zhang, G. W. Wei, Y. Wang, J. Z. Zhang, M. C. Zhang and L. Q. Shi, *Chem. Mater.*, 2008, **20**, 2144-2150.

42 W. Zhang, X. J. Lin, Y. G. Sun, D. S. Bin, A. M. Cao and L. J. Wan, *Appl. Mater. Interfaces*, 2015, **7**, 27031-27034.

43 J. Zhang, Y. Jin, C. Y. Li, Y. N. Shen, L. Han, Z. X. Hu, X. W. Di and Z. L. Liu, *Appl. Catal. B-environ.*, 2009, **91**, 11-20.

44 Dassault Systèmes BIOVIA, Materials Studio 2017, San Diego: Dassault Systèmes, 2017.

45 N. Sharifi, C. Falamaki and M. G. Ahangari, *Appl. Surf. Sci.*, 2017, **416**, 390-396.

46 A. Kumar, V. P. Kumar, A. Srikanth, V. Vishwanathan and K. V. R. Chary, *Catal. Lett.*, 2016, **146**, 35.

47 A. V. Chistyakov, P. A. Zharova, S. A. Nikolaev and M. V. Tsodikov, *Catal. Today*, 2017, **279**, 124.

48 M. Comotti, C. Della Pina, E. Falletta and M. Rossi, *Adv. Synth. Catal.*, 2006, **348**, 313-316.

49 F. Wen, W. Q. Zhang, G. W. Wei, Y. Wang, J. Z. Zhang, M. C. Zhang and L. Q. Shi, *Chem. Mater*. 2008, **20**, 2144-2150.